Ryszard GOLEMAN

Lublin University of Technology

doi:10.15199/48.2020.12.35

Performance and characteristics of a hybrid induction motor with magnetic frequency changer

Abstract. *The paper presents a model of an induction motor, supplied in three phases, in association with a magnetic frequency converter, in which a rotating field is obtained in the gap at a speed three times higher than it results directly from the frequency of the supply voltage. The equations describing its operation in the Flux 2D application are given, the results of the computer simulation are presented in the form of speed and electromagnetic torque characteristics as a function of time.*

Streszczenie. *W artykule przedstawiono model silnika indukcyjnego, zasilanego trójfazowo, w skojarzeniu z magnetycznym przetwornikiem częstotliwości, w którym uzyskuje się pole wirujące w szczelinie z prędkością trzykrotnie większą niż wynika to bezpośrednio z częstotliwości napięcia zasilającego. Podano równania opisujące jego działanie w aplikacji Flux 2D, zamieszczono wyniki symulacji komputerowej w postaci charakterystyk prędkości i momentu elektromagnetycznego w funkcji czasu. (**Działanie i charakterystyki hybrydowego silnika indukcyjnego z magnetycznym przemiennikiem częstotliwości**).*

Keywords: induction motor, magnetic frequency changer.
Słowa kluczowe: silnik indukcyjny, magnetyczny przemiennik częstotliwości.

Introduction

Continuous progress is being made in the technology of electrical machines, which is being stimulated by the availability of new construction materials, the emergence of new areas of application, the influence of power electronics, the need to save energy and new technological challenges [1, 2, 3, 4, 5]. Analysing the different structures of frequency converters and their electrical connections, it can be seen that there is a possibility to adapt them to the development of new geometric magnetic circuits for three-phase powered hybrid motors. It is possible to consider motors with the non-salient and projecting poles [6, 7, 8, 9].

In the case of motors with projecting poles and low power ratings, this is sufficient. This is also due to the technological solutions, easy adaptation and the possibility of shaping the magnetic core of the frequency converter so as to create a magnetic field of increased frequency in the air gap of the motor. In these constructions, the flux of the third harmonic produced in the converter is closed by the motor gap, which reduces its value. Better energy indicators can be obtained by modifying the structure of the magnetic circuit, creating a path of lesser reluctance for the flux of the third harmonic through the introduction of slots to accommodate the windings supplied by the converter.

The article presents the structure of a hybrid induction motor and its characteristics.

Hybrid motor structure

The stator and rotor are formed from packets of non-oriented electromagnetic sheet steel. The rotor cage is made of 28 aluminium rods. The basic element of the motor is a magnetic circuit formed from non-linear elements in which the flux is distorted (Fig. 1).

The stator's magnetic circuit has 12 saturated columns on which the frequency converter windings are placed. Four groups of columns can be distinguished, each of these groups consists of three columns, creating a system that generates third harmonic magnetic fluxes. These fluxes may be closed by columns of smaller cross-sections, which are arranged alternately with non-linear columns. The windings of the non-linear columns are powered from a three-phase mains and will form a system of two frequency converters. The windings of the frequency converters are connected in a zigzag (Fig. 2).

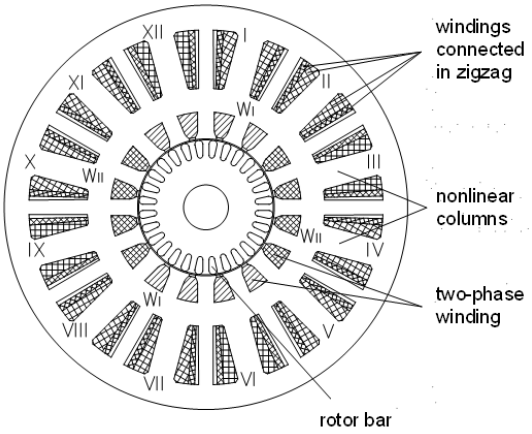

Fig.1. Cross section of a three-phase hybrid induction motor, I, II, ... XIII - non-linear columns, WI, WII - two-phase winding

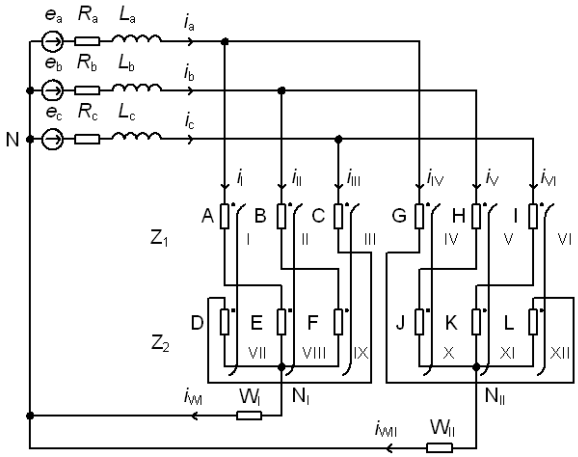

Fig.2. Wiring diagram of a three-phase hybrid induction motor, A, B, C, D, E, F and G, H, I, J, K, L - respectively the windings of the first and second frequency converter, I, II, ... XII - non-linear columns, WI, WII - bands of two-phase winding

In the corresponding columns of each transducer, the magnetic fluxes of the basic harmonic are shifted by 15^o in the first and -15^o in the second, respectively, in relation to the hypothetical flux of the system in which the windings are connected into a star. In comparison, the magnetic fluxes of the third harmonic will be shifted by 45^o and -45^o

respectively, and in relation to each other by 90° (Fig. 3). To obtain this result, the number of windings connected in a zigzag should meet the dependencies:

(1) $$\frac{z_1}{z_2}=\frac{\sin 105^o}{\sin 15^o}\cong 3{,}73$$

(2) $$\frac{z_1}{z}=\frac{\sin 105^o}{\sin 60^o}\cong 1{,}115,\quad \frac{z_2}{z}=\frac{\sin 15^o}{\sin 60^o}\cong 0{,}299$$

where: z – number of turns of a hypothetical winding, connected in a star, which provides the same level of magnetic field strength in the core as in a zigzag connection, z_1, z_2 – number of turns in sections of windings connected in a zigzag of the frequency changer.

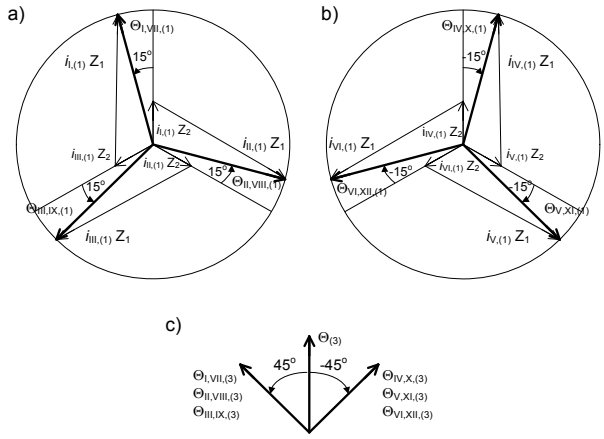

Fig.3. Magnetomotive forces generated by first harmonic currents in zigzag-connected windings, and resultant mmf ($\Theta_{\text{I,VII,(1)}}$,...) in non-linear columns of the first (a) and second (b) frequency converter, as well as magnetomotive forces of the third harmonic ($\Theta_{\text{I,VII,(3)}}$,…) in the converter columns and mmf of the hypothetical winding connected in a star ($\Theta_{(3)}$) (c)

Between the neutral points of the network and the zigzag-connected windings, there are voltages of the third harmonic

(3) $$\underline{U}_{\text{WI(3)}}=(\frac{z_1}{z}+\frac{z_2}{z})\underline{U}_{\text{W(3)}}\,e^{\text{j}\frac{\pi}{4}}$$

(4) $$\underline{U}_{\text{WII(3)}}=(\frac{z_1}{z}+\frac{z_2}{z})\underline{U}_{\text{W(3)}}\,e^{-\text{j}\frac{\pi}{4}}$$

where: $U_{\text{w(3)}}$ - voltage of the third harmonic between the neutral points of the network and a hypothetical winding connected in a star with the number of turns "z".

In 16 stator slots there is a symmetrical two-phase winding, with the number of pole pairs p = 1. Each coil has two windings. The windings of the two phases are shifted 90° to each other and connected between the neutral point of the network (N) and the neutral points of the windings connected in a zigzag (NI, NII) of the frequency converter.

Motor field-circuit equations

The equation describing the electromagnetic field in specific subareas of the motor can be expressed as

(5) $$\nabla\times(\frac{1}{\mu}\nabla\boldsymbol{A})=\boldsymbol{J}_{\text{o}}-\gamma\frac{\text{d}\boldsymbol{A}}{\text{d}t}$$

where: $\boldsymbol{A}=A_z\mathbf{1}_z$ – magnetic vector potential, $\boldsymbol{J}_{\text{o}}=J_{\text{o}}\mathbf{1}_z$ – source current density, γ – electrical conductivity, μ – magnetic permeability.

In two-dimensional motor analysis, the vectors of magnetic potential and current density have components in the z-axis direction according to the motor shaft axis. The substance derivative of the vector potential takes into account its variation in time and space, so there is no $\gamma\boldsymbol{u}\times\nabla\times\boldsymbol{A}$ component in equation (5) which contains the speed vector $\boldsymbol{u}$. In the modelled sub-areas, except for the rotor windings and bars, the right side of the equation (5) is equal to zero. The distribution of the vector potential is determined from the total current density, which can be recorded in the conductor as follows

(6) $$\boldsymbol{J}=-\gamma\frac{\text{d}\boldsymbol{A}}{\text{d}t}+\gamma\frac{u}{l_{\text{p}}}\mathbf{1}_{\text{a}}$$

where: u – voltage between conductor ends, l_{p} – length of conductor.

As the magnetic field disappears outside the engine stator, the Dirichlet's boundary condition is assumed to be zero on a circle at some distance from its surface ($A_z = 0$). An analogous condition occurs on the axis of the coordinate system, which is the axis of rotation of the rotor.

The equations of the stator circuit, taking into account the voltage of the three-phase mains supply, are coupled with the equations of the electromagnetic field. For example, one of them, formulated on the basis of the Kirchhoff voltage law, for frequency converter circuits and the stator segment in which the two-phase motor winding is located, has the form

(7) $$e_{\text{a}}=R_{\text{a}}i_{\text{a}}+L_{\text{a}}\frac{\text{d}i_{\text{a}}}{\text{d}t}+(R_{\text{z1A}}+R_{\text{z2E}})i_{\text{I}}+\frac{\text{d}\Psi_{\text{A}}}{\text{d}t}+\frac{\text{d}\Psi_{\text{E}}}{\text{d}t}+R_{\text{WI}}i_{\text{WI}}+\frac{\text{d}\Psi_{\text{WI}}}{\text{d}t}+R_{\text{WIcz}}i_{\text{WI}}+L_{\text{WIcz}}\frac{\text{d}i_{\text{WI}}}{\text{d}t}$$

where: R_{a}, L_{a} – resistance and inductance of power line conductors, R_{z1A}, R_{z2E} – resistances of frequency converter winding sections, R_{WIcz}, L_{WIcz} – resistance and end-connection leakage inductance of a two-phase winding, Ψ_{A}, Ψ_{E} – linkage fluxes of windings sections connected in a zigzag, Ψ_{WI}, – linkage flux of a two-phase winding section.

The above set of equations shall be completed by taking into account the equations for the current balance at the stator circuit nodes

() $$\begin{aligned}&i_{\text{a}}+i_{\text{b}}+i_{\text{c}}=0\\&i_{\text{I}}+i_{\text{II}}+i_{\text{III}}=i_{\text{WI}}\\&i_{\text{IV}}+i_{\text{V}}+i_{\text{VI}}=i_{\text{WII}}\\&i_{\text{a}}=i_{\text{I}}+i_{\text{IV}}\\&i_{\text{b}}=i_{\text{II}}+i_{\text{V}}\end{aligned}$$

where: J – current density, r – distance, A,B,C – coefficients.

The magnetic flux linked to the windings can be expressed by vector potential

(9) $$\Psi=\frac{l\,z}{S}\iint_{\text{S}}\boldsymbol{A}\cdot\text{d}\boldsymbol{S}$$

where: l – core length, z – number of coil turns, S – cross-sectional area of the winding.

An equivalent rotor circuit is shown in Fig. 4. The rotor cage bars are represented by R_{b} resistances, resulting from their cross-sectional area and length, and by sources of induced voltage e_{n}. Rings that connect bars are represented by series-connected elements representing the resistance R_{r} and the leakage inductance of the ring section L_{r}.

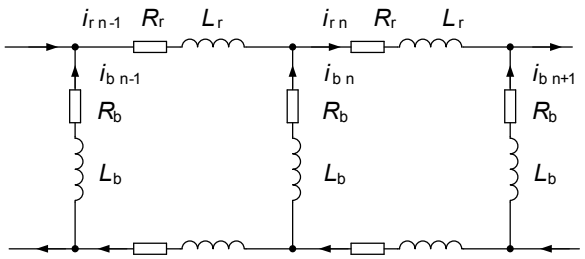

Fig.4. Electrical circuit scheme of the rotor section

For a section of the rotor circuit, the equations resulting from Kirchhoff's laws are

$$e_{\mathrm{n}} - e_{\mathrm{n-1}} + R_{\mathrm{b}} i_{\mathrm{bn}} - R_{\mathrm{b}} i_{\mathrm{bn+1}} + 2 i_{\mathrm{rn}} R_{\mathrm{r}} + 2 L_r \frac{\mathrm{d}i_{\mathrm{rn}}}{\mathrm{d}t} = 0 \tag{10}$$

$$i_{\mathrm{bn}} = i_{\mathrm{rn}} - i_{\mathrm{rn\text{-}1}}$$

where: J – current density, r – distance, A,B,C – coefficients.

The electromotive force induced in the rotor bar is

$$e_{\mathrm{n}} = -\frac{l_{\mathrm{b}}}{S_{\mathrm{b}}} \frac{\mathrm{d}}{\mathrm{d}t} \iint_S \boldsymbol{A} \cdot \mathrm{d}\boldsymbol{S} \tag{11}$$

where: l_{b} – rotor bar length, S_{b} – cross-section of the rotor bar.

The equation of the rotor's motion can be expressed as follows

$$J \frac{\mathrm{d}\omega}{\mathrm{d}t} = T_e - k\omega - T_o \tag{12}$$

where: J – inertial momentum of the rotor, ω – angular velocity, T_{e} – electromagnetic torque, T_{o} – load torque, k – friction constant.

Equation (5), with the application of Flux 2D, is solved by means of successive time steps in the areas to be discredited, in the system of coordinates related to the stator and rotor. The finite element mesh in the motor gap is reproduced in each step, due to the rotor's rotational movement. The electromagnetic torque of the engine was calculated on the basis of the change in the magnetic energy W of the system with respect to the small angular displacement θ of the rotor

$$T_e = -\frac{\partial W}{\partial \theta} \tag{13}$$

Electromagnetic field and dynamic characteristics

To determine the electromagnetic field in the cross-section of the motor model and the instantaneous currents and voltages as well as torque and speed, the finite element method was used, Flux 2D software was applied. The motor section sub-areas were discredited, creating a finite element mesh containing 8534 elements and 17137 nodes. The finite element mesh for the sectional area of the motor model covering the rotor and stator slot zone and the air gap is shown in Fig. 4. It was assumed that the magnetic circuit of the motor was made of PE-23 generator sheets, 0.5 mm thick, the length of the package is 25 mm and its diameter is 90 mm. The motor was supplied from a three-phase voltage source with a sinusoidal waveform and a 220 V rms value of the phase voltage. Tables 1 and 2 show the winding and rotor parameters which were determined from the analytical formulas and accepted for analysis. The calculations were made for the unloaded motor. The distributions of magnetic induction is shown in Fig. 6 .

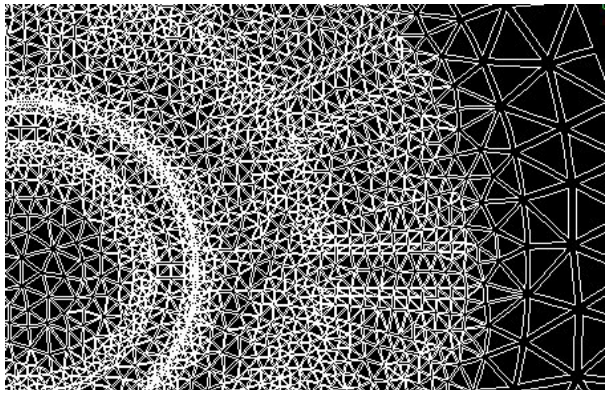

Fig.5. Finite element mesh for a section of the motor model

Table 1. Winding parameters

Winding sections connected in a zigzag	Two-phase winding
Resistance R_{Z1} = 22,81 Ω R_{Z2} = 7,06 Ω	Resistance R_w = 20,16 Ω
Number of turns Z_1 = 3071 Z_2 = 823	Number of turns Z_2 = 950 Number of slots 16

Table 2. Rotor parameters

Rotor cage	Rotor rings	Rotor
Resistivity ρ = 3,23×10^{-8} Ω m	Leakage inductance of the ring sector L_r 1×10^{-9} H	Length l = 25×10^{-3} m Diameter 30 mm
Number of bars 28	Resistance of the ring sector R_r = 4,05×10^{-6} Ω	Moment of inertia J = 9,18×10^{-6} kg·m

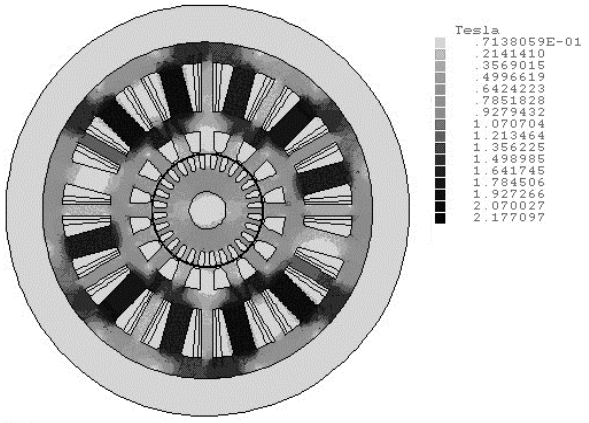

Fig.6. Magnetic induction in the cross-section of the motor's magnetic circuit, at a time 0.085 s

The instantaneous magnetic induction values in non-linear stator columns reach values above 2 T, while in the rotor area about 1 T. Source currents are the sum of the currents of both frequency multiplier systems and include a smaller proportion of higher harmonics than the currents in the converter windings. The characteristics of rotational speed, electromagnetic torque as well as the mechanical characteristics, under no load and in a system without capacitors and with capacitors connected in parallel to a two-phase winding, are shown in Figs 7, 8 and 9.

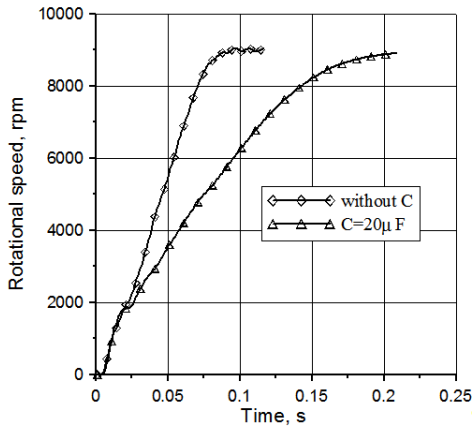

Fig.7. Rotor speed as a function of time at no-load condition

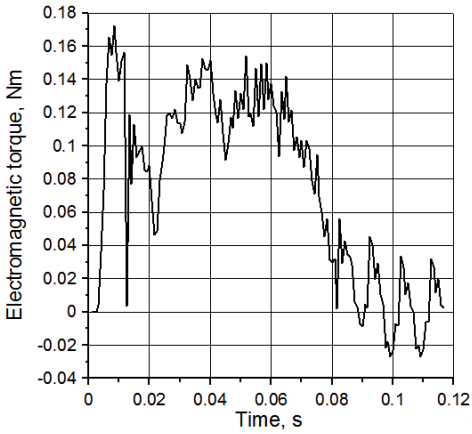

Fig.8. Electromagnetic torque as a function of as a function of time (without capacitors)

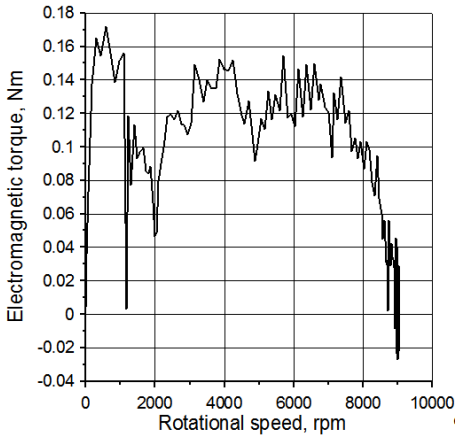

Fig.9. Electromagnetic torque as a function of rotational speed (without capacitors)

Conclusion

The model of the motor with magnetic frequency changer uses the third harmonic of the magnetic flux and enables to reach the rotational speed nearly 9000 rpm at mains 50Hz.

At the magnetic circuit of the outer part of the stator at the adequate winding connections, the three phase flux system of 50Hz is transformed into the two-phase of 150Hz, that take place among the neutral point of the network and the neutral points of the windings connected in the zigzag.

The speed increases linearly over a significant period of time. In the initial start-up phase, and only at speeds close to synchronous, the speed increases are smaller. In the interval from 0.01 s to 0.03 s there is a noticeable influence of the first harmonic magnetic induction and spatial harmonics of the field in the air gap on the shape of the characteristics.

The connection of capacitors between the mains neutral point and the neutral points of the zigzag-connected winding sections causes a voltage change between these points during the motor start and in steady state. This makes it possible to influence the shape of the speed and torque characteristics.

With capacitor values (C = 10 μF and above), the slope of the rotor speed characteristics decreases, thus increasing the starting time.

The electromagnetic torque of the motor increases during the initial starting phase, then reaches values lower than in a configuration without capacitors.

Hybrid motor calculations by classical methods are very complex and give significant errors due to the non-linearity of the magnetic circuit. The use of numerical coupled circuit-field calculations allows for the analysis of the transient states of this motor.

***Author**: dr hab. inż. Ryszard Goleman, Politechnika Lubelska, Wydział Elektrotechniki i Informatyki, ul. Nadbystrzycka 38a, 20-618 Lublin, E-mail: r.goleman@pollub.p*

REFERENCES

[1] Buticchi G. at all, Challenges of the optimization of a high-speed induction machine for naval applications, *Energies*, (2019), 12, 2431

[2] Gieras J. F., Advancements in electric machines, Springer, 2008

[3] Ravi Prakash, Mohammad Junaid Akhtar, Behera R. K., Parida S. K., Design of a Three Phase Squirrel Cage Induction Motor for Electric Propulsion System, T*hird International Conference on Advances in Control and Optimization of Dynamical Systems*, March 13-15, 2014. Kanpur, India

[4] Sobczyński D., Review of solutions used in high-speed induction motor drives operating in household appliances, *Power Electronics And Drives*, Vol. 1(36), No. 1, 2016

[5] Soong W.L., Kliman G.B., Johnson R.N., White R.A., Miller J.E., Novel high-speed induction motor for a commercial centrifugal compressor, *IEEE Trans. on Industry Applications*, vol. 36, No. 3, 2000, pp. 706 -713

[6] Sakamoto Y., Ohkubo T., Ohta M., Natsusaka M., Three-phase parametric induction motor excited by a single-phase power supply, *IEEE Trans. Magn*., 37 (2001), No. 4, pp.2837-2839

[7] Yamada S., Takeuchi A., Sudani T., Bessho K., High-speed ac motor including the function of a magnetic frequency tripler", *IEEE Trans. Magn*., 22 (1986), No. 5, pp. 967-969

[8] Goleman R., Three phase induction motor integrated with a magnetic frequency changer, *Journal of Magnetism and Magnetic Materials*, 254-255, 2003, pp. 229-301

[9] Goleman R., Basic properties of a single-phase hybrid motor prototype, *Journal of Magnetism and Magnetic Materials*, vol. 159, No.3, 1996, , pp.75-76